中国光学（中英文） Chinese Optics 核心期刊

Low-noise linear-polarization fiber laser with polarization adjusted parity-time symmetry in a linear reflection structure

LIN Zi-han, CAO Zhi-gang, CHEN Jia-ming, FANG Chong-xu, CHENG Rui, WANG Xing-yun, WANG Xu, LIU Peng, CAO Jian-bo, LIN Ji-ping

Citation:
LIN Zi-han, CAO Zhi-gang, CHEN Jia-ming, FANG Chong-xu, CHENG Rui, WANG Xing-yun, WANG Xu, LIU Peng, CAO Jian-bo, LIN Ji-ping. Low-noise linear-polarization fiber laser with polarization adjusted parity-time symmetry in a linear reflection structure[J]. *Chinese Optics*, In press. doi: 10.37188/CO.EN-2026-0009
蔺子翰, 曹志刚, 陈家铭, 方崇旭, 程瑞, 王幸运, 汪旭, 刘鹏, 曹剑波, 林继平. 线性反射结构中基于偏振调控宇称-时间对称的低噪声线偏振光纤激光器[J]. 中国光学, 优先发表. doi: 10.37188/CO.EN-2026-0009

View online: https://doi.org/10.37188/CO.EN-2026-0009

Articles you may be interested in

Widely-wavelength-tunable brillouin fiber laser with improved optical signal-to-noise ratio based on parity-time symmetric and saturable absorption effect
基于宇称时间对称与饱和吸收效应的宽可调谐高光信噪比布里渊光纤激光器
Chinese Optics. 2024, 17(5): 1244 https://doi.org/10.37188/CO.EN-2024-0016

Low-noise wide tuning -nm DBR narrow-linewidth single-frequency fiber laser
低噪声宽调谐 nm分布式布拉格反射窄线宽单频光纤激光器
Chinese Optics. 2025, 18(6): 1289 https://doi.org/10.37188/CO.2025-0071

Output characteristics of an all-fiber laser with a 2- μ m MOPA structure
2- μ m MOPA结构全光纤激光器输出特性研究
Chinese Optics. 2023, 16(2): 399 https://doi.org/10.37188/CO.2022-0191

Key technology analysis and research progress of high-power narrow linewidth fiber laser based on the multi-longitudinal-mode oscillator seed source
基于多纵模振荡种子源的高功率窄线宽光纤激光器关键技术分析及研究现状
Chinese Optics. 2024, 17(1): 38 https://doi.org/10.37188/CO.2023-0074

Laser Doppler velocimetry with a dual polarization structure
双路偏振结构的激光多普勒测速系统
Chinese Optics. 2023, 16(4): 753 https://doi.org/10.37188/CO.2022-0211

Polarization-multiplexing of a laser based on a bulk Yb:CALGO crystal
基于Yb:CALGO晶体激光器的偏振复用
Chinese Optics. 2023, 16(6): 1475 https://doi.org/10.37188/CO.EN-2023-0005

文章编号　2097-1842(xxxx)x-0001-15

Low-noise linear-polarization fiber laser with polarization adjusted parity-time symmetry in a linear reflection structure

LIN Zi-han, CAO Zhi-gang*, CHEN Jia-ming, FANG Chong-xu, CHENG Rui, WANG Xing-yun, WANG Xu, LIU Peng, CAO Jian-bo, LIN Ji-ping

(*State Key Laboratory of Opto-Electronic Information Acquisition and Protection Technology*, *School of Optoelectronic Science and Engineering*, *Anhui University*, 230601 *Hefei*, *China*; *Key Laboratory of Opto-Electronic Information Acquisition and Manipulation of Ministry of Education*, *Anhui University*, 230601 *Hefei*, *China*)

* *Corresponding author*, *E-mail*: *caozhigang@ahu.edu.cn*

Abstract: A low-noise linear-polarization single longitudinal mode (SLM) fiber laser based on polarimetric parity-time (PT) symmetry is proposed and experimentally demonstrated. PT symmetry is achieved within a linear reflection structure. When the balanced gain–loss contrast surpasses the coupling coefficient, the condition for PT-symmetry breaking is met, enabling the realization of an SLM laser. Stable laser output with a high sidemode suppression ratio (SMSR) of 62.6 dB and a high optical signal-to-noise ratio (OSNR) of 64.32 dB is realized. The Lorentz linewidth is measured as 182.5 Hz. The degree of polarization (DOP) and polarization extinction ratio (PER) of the laser remain above 99.8 % and 30.8 dB within 4 hours. Furthermore, the relative intensity noise (RIN) and phase noise of the PT-symmetric laser are analyzed and compared with those of fiber lasers and semiconductor lasers. The results demonstrate the low-noise performance of the proposed PT-symmetric laser.

Key words: Parity-time symmetry; linear reflection structure; single longitudinal mode; fiber laser.

收稿日期:xxxx-xx-xx; **修订日期**:xxxx-xx-xx

基金项目:国家重点研发计划资助项目(No. 2024YFE03000200, No. 2016YFC0301900, No. 2016YFA0301901); 国家自然科学基金(No. 61605001)

Supported by National Key R & D Program of China under Grant (No. 2024YFE03000200, No. 2016YFC0301900, No. 2016YFC0301901); National Natural Science Foundation of China (No. 61605001).

线性反射结构中基于偏振调控宇称-时间对称的低噪声线偏振光纤激光器

蔺子翰, 曹志刚*, 陈家铭, 方崇旭, 程　瑞, 王幸运, 汪　旭, 刘　鹏, 曹剑波, 林继平
（安徽大学 光电科学与工程学院 光电信息获取与防护技术全国重点实验室, 安徽 合肥 230601;
安徽大学 光电信息获取与控制教育部重点实验室, 安徽 合肥 230601）

摘要: 为了能在更简化的结构设计中实现更稳定的宇称-时间(parity-time, PT)对称, 以提高光信噪比和边模抑制比, 本文提出并实验验证了一种基于偏振调控 PT 对称的低噪声线偏振单纵模光纤激光器。该 PT 对称结构采用线性反射结构, 由工作在慢轴上的保偏环形器、偏振控制器以及单模光纤布拉格光栅组成。当增益和损耗相等且超过耦合系数时, 系统满足 PT 对称破缺条件, 从而实现单纵模激光输出。实验结果与理论分析结果一致。激光器获得了稳定输出, 其边模抑制比达到 62.6 dB, 光信噪比为 64.32 dB, 洛伦兹线宽为 182.5 Hz。在 4 h 测试时间内, 激光器的偏振度和偏振消光比分别保持在 99.8% 和 30.8 dB 以上。此外, 对 PT 对称激光器的相对强度噪声和相位噪声进行了分析, 并与其他光纤激光器和半导体激光器进行了对比, 验证了 PT 对称激光器的低噪声特性。

关　键　词: 宇称时间对称; 线性反射结构; 单纵模; 光纤激光器.
中图分类号: TN248　　**文献标志码:** A　　**doi:** 10.37188/CO.EN-2026-0009　　**CSTR:** 32171.14.CO.EN-2026-0009

1 Introduction

Single-longitudinal-mode (SLM) lasers are widely applied in various fields, such as lidar[1], microwave photonics[2-3], coherent optical communication[4-5], spectroscopy[6], and precision measurement[7-8], due to their advantages of high coherence, narrow linewidth, and so on. Therefore, to realize SLM operation, several approaches have been proposed, including ultrashort cavities[9], saturable absorbers[10], composite cavities[11], and self-injection locking[12].

In recent years, parity-time (PT) symmetry in non-Hermitian optics has introduced a novel approach for achieving mode selectivity in fiber lasers. A method proposed by Li et al. in 2020 is presented. Two subspaces are formed in the ring loop by using two polarizers and two polarization controllers (PC). The gain and loss in the loop will be adjusted by the PCs to achieve PT symmetry and SLM output[13]. In the subsequent studies, the mode selection effect of PT symmetry is achieved by changing the loop structure[14-16]. However, when PT symmetry is achieved through a ring structure with a main loop, the precise tuning of gain and loss modes requires the cooperation of multiple optical devices, making the conditions for achieving PT symmetry more stringent. Based on the aforementioned measurements, the laser fails to simultaneously achieve an optical signal-to-noise ratio (OSNR) and a side-mode suppression ratio (SMSR) both exceeding 50 dB. Therefore, it is essential to explore alternative structures for achieving higher OSNR and SMSR. An alternative approach was proposed by Zhang et al. in 2023. In the double ring cavity, the PT-symmetry breaking is realized by using double rings with different lengths, with the SMSR enhanced to 53 dB[17]. However, the double loop structure necessitates the coupling of two precisely matched optical loops, and then it is imperative to individually regulate the gain and loss loops to attain PT symmetry. Alternatively, an approach incorporates the assistance of stimulated Brillouin scattering (SBS) to realize PT symmetry, which can enhance the OSNR to approximately 60 dB, while the SMSR only reaches 33 dB. A significant drawback of this specific technique, however, is that it im-

poses stricter requirements on the pump source, leading to increased structural complexity and cost in practical applications[18-19]. Therefore, it is highly desirable to achieve more stable PT symmetry within a simplified structural design for the enhancement of SMSR and OSNR. More importantly, the noise performance of PT-symmetric SLM lasers remains insufficiently understood, and direct comparisons with other SLM laser technologies are still limited.

In this paper, we propose and experimentally demonstrate a PT-symmetric low-noise linear-polarization SLM fiber laser based on polarization mode manipulation. The proposed structure simplifies cavity adjustment while supporting stable polarization states. Additionally, the linear reflection structure provides good mutual coupling and consistent responses to environmental disturbances, which are conducive to achieving PT symmetry. By setting the pump power to 150 mW, the SMSR and OSNR are measured to be 62.6 dB and 64.32 dB, respectively. The fluctuations in SMSR, central wavelength, and power remain below 1.5 dB, 0.02 nm, and 0.1 dB within 4 hours. The laser maintains a high polarization extinction ratio (PER) of over 30 dB, indicating that it can maintain a stable linearly polarized state. The Lorentz linewidth is measured as 182.5 Hz. When compared with other fiber lasers and semiconductor lasers, the proposed laser demonstrates significantly superior performance in both relative intensity noise (RIN) and phase noise. Finally, to achieve a tunable SLM laser, the SM-FBG is replaced with a single-mode fiber mirror, and a polarization-maintained tunable optical bandpass filter (PM-TOBPF) is incorporated into the main cavity. The laser wavelength is tunable over 1 516–1 575 nm, corresponding to a 59 nm tuning range. Owing to its narrow linewidth, high SMSR, stable linear polarization, and low-noise characteristics, the proposed PT-symmetric fiber laser provides a promising laser source for applications requiring stable SLM operation. Potential application areas include coherent detection, microwave photonics, lidar, interferometric sensing, and precision optical measurement. Moreover, the relatively simple linear reflective structure is advantageous for the practical implementation of fiber laser systems.

2 Theoretical analysis

A linear reflection structure is constructed using a polarization-maintaining circulator (PM-CIR) operating along the slow axis, a PC and a single-mode fiber Bragg grating (SM-FBG). The structure is utilized to realize the PT-symmetric system, as illustrated in Fig. 1(a). In the structure, two orthogonal polarized lights generated by the birefringent effect are controlled to build two PT-symmetric loops. One of the polarimetric loops supports the gain mode, while the other supports the loss mode. The PC precisely adjusts the gain and loss coefficients of the two polarization loops, thereby establishing PT symmetry. The SM-FBG determines the laser wavelength and performs the initial filtering.

The fiber-optic PC with three adjustable paddles adopts a triple-layer configuration, where a half-wave plate is placed between two quarter-wave plates in a symmetric configuration, allowing precise manipulation of the polarization state via successive phase retardation. The transfer function of the three-paddle PC is given by[20]:

$$F_{PC}=\begin{bmatrix}\exp(i\phi_2) & 0\\ 0 & 1\end{bmatrix}\times\begin{bmatrix}\cos\theta & -\sin\theta\\ \sin\theta & \cos\theta\end{bmatrix}\times\begin{bmatrix}\exp(i\phi_1) & 0\\ 0 & 1\end{bmatrix}, \quad (1)$$

where ϕ_1 and ϕ_2 are the phase retardance introduced to the two orthogonally polarized light waves by the two quarter-wave plates, and θ is the rotation angle of the polarization direction introduced by the half-wave plate. When the PC is adjusted, the birefringence effect introduces a relative phase delay between the two orthogonal polarization modes. The half-wave plate and quarter-wave plate have different effects on the construction of PT symmetry.

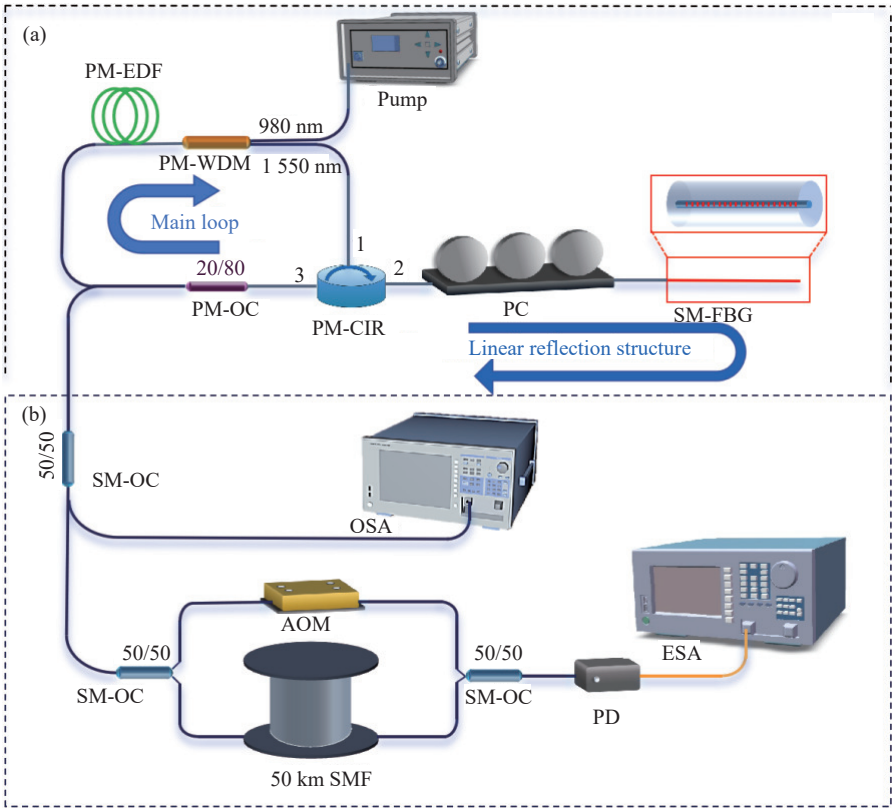

Fig. 1 (a) Experimental setup. (b) Optical spectrum measurement system and delayed self-heterodyne (DSH) system. (PM-EDF: polarization-maintaining erbium-doped fiber, PM-WDM: polarization-maintaining wavelength-division multiplexer, PM-OC: polarization-maintaining optical coupler, SM-OC: single-mode optical coupler, AOM: acousto-optic modulator, PD: photodiode, SMF: single-mode fiber).

For one thing, the eigenfrequencies between the two loops need to be matched to achieve PT symmetry. The PT-symmetric condition is satisfied when the eigenfrequency separation $\delta\omega_n$ equals zero, where $\delta\omega_n = \dfrac{(\phi_x - \phi_y)\mathrm{c}}{n_{eff}(L+2L_0)}$. ϕ_x and ϕ_y is the phase of the two orthogonal polarized lights produced by the birefringence, c represents the speed of light in vacuum., n_{eff} is the effective refractive index, L and L_0 are the fiber lengths of the main loop cavity and linear reflection structure, respectively. The quarter-wave plate of PC needs to be adjusted to make the values of $\phi_x$andϕ_y equal. The adjustment angle of the quarter-wave plate is defined as θ_a. Therefore, θ_a can be adjusted to align between the real parts of the eigenfrequencies so as to establish PT symmetry[21], as illustrated in Fig. 2(a).

For another, adjusting the half-wave plate in the PC can alter the polarization direction of two orthogonal polarized lights. The slow axis of the PM-CIR is defined as the principal optical axis. Assuming that the slow and fast polarization lights generated by the birefringence effect are $E_x$and E_y, respectively, the angle between the principal optical axis and the slow polarized light E_x is defined as θ_b, as shown in Fig. 2(b). By adjusting θ_b with the half-wave plate, the round-trip gain, loss, and coupling coefficient of the two polarization loops can be tuned. Therefore, PT symmetry is established under the condition that the imaginary parts of the eigenfrequencies in the two polarimetric loops are equal.

The polarization state evolution in the linear reflection structure is shown in Fig. 2(b). When the light passes through the PM-CIR, a linearly polarized light is generated and operates on the slow axis (the principal optical axis), which is defined as state 1. When passing through the PC, two orthogonal polarized lights E_x and E_y are generated, and the angle

of θ_b can be adjusted by a half-wave plate, which is defined as state 2. When the reflected light passes through the PC again, a portion of the polarized lightE_x couples with the other polarized light E_y, and the same coupling occurs in reverse, which is defined as state 3. When returning to the PM-CIR, only the components of the two polarized lights on the principal optical axis can pass through the PM-CIR, which is defined as state 4. Therefore, the PT-symmetric system can be realized by controlling the PC. Furthermore, the polarization state remains invariant within the polarization-maintaining main ring cavity. As a result, the PT-symmetric system can operate with minimal initial loss.

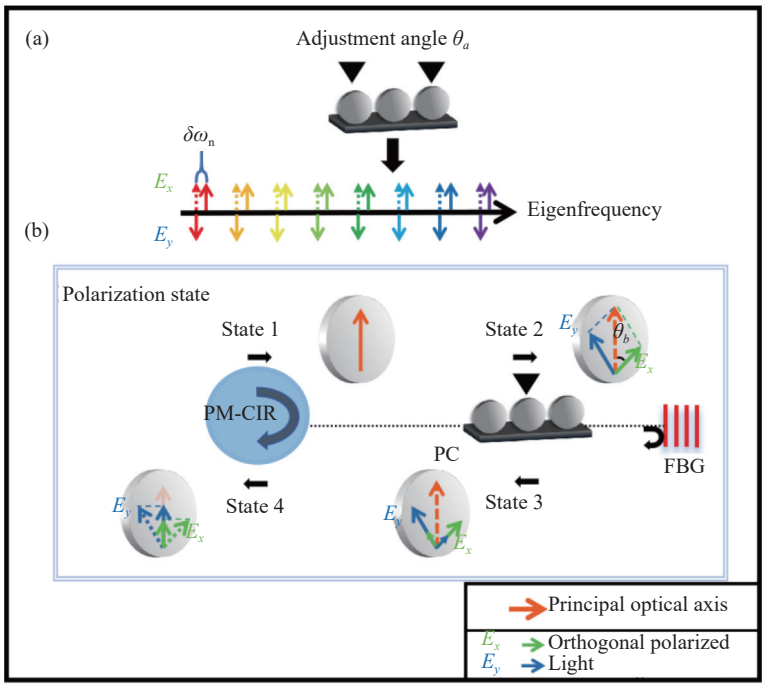

Fig. 2 (a) The alignment of the real part of the eigenfrequency between the polarimetric loops when the phase delay is tuned by the variation of θ_a. (b) The polarization state evolution in the linear reflection structure when the gain and loss of two orthogonal polarized lights are tuned by the variation of θ_b.

It should be noted that the slow and the fast polarization lights of the electric field $E(t)$ are E_x andE_y, the coupled mode equation of two orthogonal polarimetric loops is given by:

$$\frac{d}{dt}\begin{bmatrix} E_x \\ E_y \end{bmatrix} = \begin{bmatrix} -i\omega_n + g & i\kappa \\ i\kappa & -i\omega_n + l \end{bmatrix}\begin{bmatrix} E_x \\ E_y \end{bmatrix} \quad , \quad (2)$$

where $\omega_n$is the frequency of the n-th eigenmode of the ring cavity. g and $l$are respectively the gain or loss of the mode in the two polarimetric loops, and κ denotes the coupling coefficient between the two polarization loops. According to the definition of unit time gain and loss, the gain and loss are given by:

$$g = \ln g_x / \mathrm{T} \quad , \quad (3)$$

$$l = \ln g_y / \mathrm{T} \quad , \quad (4)$$

where g_x and g_y are the round-trip gain and loss coefficient, T is the round-trip time of the cavity. When the polarization light $E_x$and E_y are recirculated in the loop, the angles between the two orthogonal polarized lights with the principal optical axis will lead to different round-trip gains coefficient and coupling coefficient in the two orthogonal polarization loops, given by:

$$g_x = g_0 \cos^2\theta_b \quad , \quad (5)$$

$$g_y = g_0 \sin^2\theta_b \quad , \quad (6)$$

$$\kappa = g_0 \sin\theta_b \cos\theta_b \quad , \quad (7)$$

where g_0 is the round-trip gain of the electric field.

When the gain matches the loss in the two coupled loops, it means that $g=-l=v_n$. v_n is the balance value between gain and loss. Equation (2) can be solved:

$$\omega_n^{1,2}=\omega_n\pm\sqrt{\kappa^2-v_n^2}\quad , \tag{8}$$

The loop achieves the balance of gain and loss, that is $g_x g_y=1$. Then it can be calculated that the polarization rotation angle to realize the PT symmetry of the imaginary part of the eigenfrequencies is:

$$\theta_g=\pm\frac{1}{2}\arcsin\left(\frac{2}{g_0}\right)\quad , \tag{9}$$

Based on the above analysis, when the gain and loss in the two cavities are balanced and remain below the coupling coefficient κ, each resonant frequency encounters an equal amount of gain and loss. As a result, the mode oscillation is maintained near the laser threshold. Once v_n exceeds κ, the mode reaches the PT-symmetry breaking region. Consequently, $\omega_n^{1,2}$ becomes a complex number. The real part of its resonant frequency remains equal, while the imaginary part splits. This indicates that the mode exhibits either gain or loss. Specifically, by adjusting the reasonable coupling coefficient or gain/loss value, modes that do not reach the lasing threshold are suppressed, which is conducive to achieving single mode amplification output.

For a conventional laser system, the gain difference between the primary mode and the second-highest mode is defined as g_{max}. And for the PT-symmetric system is defined as g_{max}^{PT}, which are given separately:

$$g_{max}=g_1-g_2\quad , \tag{10}$$

$$g_{max}^{PT}=\sqrt{g_1^2-g_2^2}\quad , \tag{11}$$

Here g_1 is the gain of the primary mode, g_2 is the gain of the second highest mode. Then the gain contrast ratio R can be expressed as:

$$R=\frac{g_{max}^{PT}}{g_{max}}=\sqrt{\frac{g_1/g_2+1}{g_1/g_2-1}}\quad , \tag{12}$$

The gain can be amplified by a factor of R when g_1 exceeds g_2. Notably, the gain contrast exhibits dramatic enhancement as g_2 approaches g_1. Consequently, the primary mode exhibits gain enhancement in the condition of PT-symmetry breaking, leading to more stable and better mode selection.

3 Theoretical verification and results

To verify the function of the linear reflection structure, an experimental setup is built to show the polarization-dependent loss tuning, as depicted in Fig. 3. Two linearly polarized lasers with perpendicular polarized directions are used in the experiment. For the convenience of distinguishing orthogonal polarized lasers, the two lasers have different wavelengths. The orthogonally polarized lights are combined using a polarization beam combiner (PBC) and injected into the linear reflection structure by a SM-OC. The single-mode fiber mirror ensures the reflection of both polarized lasers. The output spectra of the linear reflection structure are monitored at port 3 of the PM-CIR using the optical spectrum analyzer (OSA). When the PC is adjusted, the variations in polarization-dependent loss can accordingly be measured by monitoring power variations at different wavelengths.

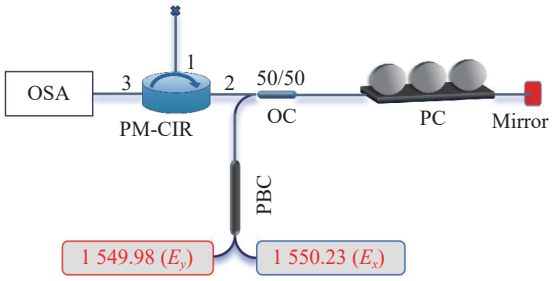

Fig. 3 The experimental setup for verifying the tuning of polarization-dependent loss.

When there is no PC in the experimental setup, the output spectrum indicates that the powers of the two lasers are virtually identical, as depicted in Fig. 4.

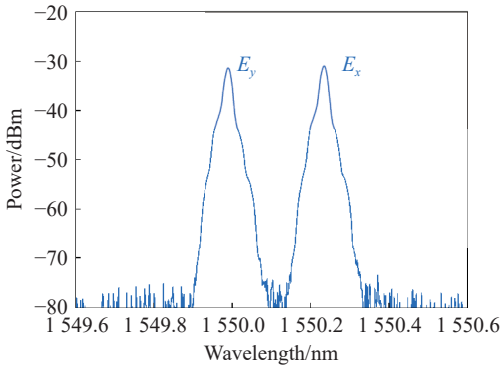

Fig. 4 The output optical spectrum without using a PC in the experimental setup.

Then, in the complete validation experimental setup, the initial angle of θ_b is set to 45°. Meanwhile, the light power changes periodically as the PC adjusts its angle. Thus, the adjustment range for a single period is set to 0° to 90°. By adjusting the half-wave plate, the power changes of the two lasers differ, indicating that the losses of E_x and E_y polarization modes are different, respectively, as shown in Fig. 5(a) and Fig. 5(b). When rotated clockwise, the power of the laser at 1 549.98 nm, which is the fast polarization component (E_y), decreases. Simultaneously, the power of the laser at 1 550.23 nm, which is the slow polarization component (E_x), increases. The changes in the power of the two lasers are shown in Fig. 6. These results confirm that the designed structure forms two orthogonal polarization loops with different losses.

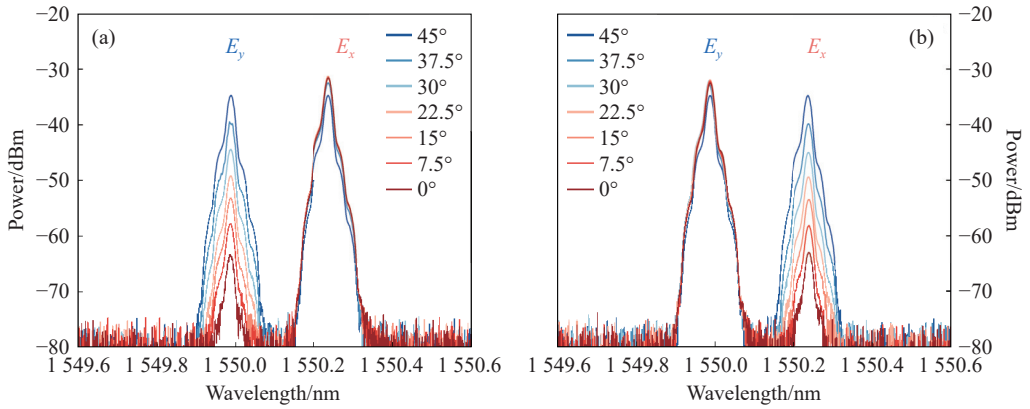

Fig. 5 The optical spectra under different half-wave plate adjustments (θ_b). (a) Adjustment from 0° to 45°. (b) Adjustment from 45° to 90°.

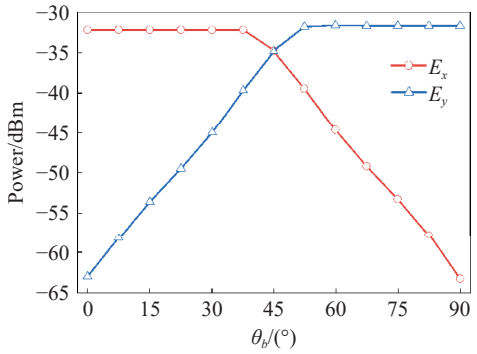

Fig. 6 The evolution of the power of the two lasers at different θ_b.

4 Experimental setup and results

As shown in Fig. 1(a), the low-noise linear-polarization fiber laser with polarization adjusted PT symmetry in the linear reflection structure is constructed in the experiment. A 10 m PM-EDF (IXF-EDF-FGC-980-PM, iXblue) is used as the gain medium. A 976 nm semiconductor laser serves as the pump, and pump light is injected into the cavity using a PM-WDM. A PM-CIR and a SM-FBG constitute the linear reflection structure. The SM-FBG, with a central wavelength of 1 550.20 nm and a bandwidth of 0.09 nm, can roughly select the laser wavelength. The PC provides control over the gain–loss coefficients of the two polarization loops. A 20/80 polarization-maintaining optical coupler (PM-OC) is utilized for laser output. All the PM devices operate on the slow axis. The length of the

ring cavity is about 26 m. The laser output is divided into two parts by the SM-OC for the next performance test. As shown in Fig. 1(b), one part is launched to the OSA, and the other part is used for mode analysis and linewidth measurement by the DSH method. The frequency shift of the AOM is 100 MHz, and the length of the delayed fiber is 50 km. A PD is placed after the recombination of the two light beams to detect the beat spectrum centered at 100 MHz, utilizing an electrical spectrum analyzer (ESA).

4.1 Frequency spectrum

To validate the efficiency of mode suppression in the designed PT-symmetric SLM laser, the PC is initially adjusted to create an imbalance between the gain and loss of the two loops. When the pump power reaches 8 mW, the laser begins to oscillate. When the pump power is increased to 150 mW, multimode laser operation is observed in the measured electrical spectrum, with a measurement bandwidth of 100 MHz and a resolution of 100 Hz, as shown in Fig. 7(a). The free spectral range (FSR) is 7.97 MHz. Within the bandwidth of the SM-FBG (0.09 nm, approximately 11.25 GHz), about 1411 longitudinal modes are oscillating.

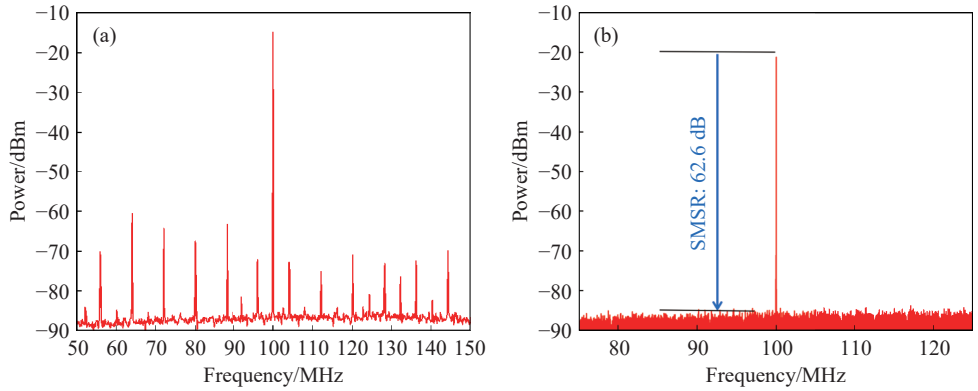

Fig. 7 The radio frequency spectra of the beat signals (a) The system is operating without PT-symmetry breaking. (b) The system is operating with PT-symmetry breaking.

Then, the gains and losses of the two loops are precisely adjusted through the PC, ensuring balanced operation and driving the gain–loss contrast to surpass the coupling coefficient, which results in PT-symmetry breaking. Thus, the dominant mode reaches the PT-symmetry breaking region to obtain additional gains, while other side modes are suppressed. An SMSR of 62.6 dB is obtained, demonstrating efficient mode suppression enabled by PT symmetry, as shown in Fig. 7(b).

When the pump power varies, the designed laser can still achieve PT-symmetry breaking, allowing the output laser to maintain SLM operation. The effect of pump power on the SMSR is also analyzed, as shown in Fig. 8. As the power increases from 10 mW to 150 mW, the SMSR experiences an increase, rising from 33.7 dB to 62.6 dB, as can be seen in the inset of Fig. 8.

As shown in Fig. 9, the SLM laser output is monitored for 4 hours when the pump power is set to 150 mW. The dominant mode, which satisfies the PT-symmetry breaking condition, always maintains an SMSR of 63 dB with fluctuations of less than 1.5 dB, demonstrating high stability, as shown in the inset of Fig. 9. All stability measurements are carried out under normal laboratory conditions on a standard optical table, without active temperature control or dedicated vibration-isolation packaging.

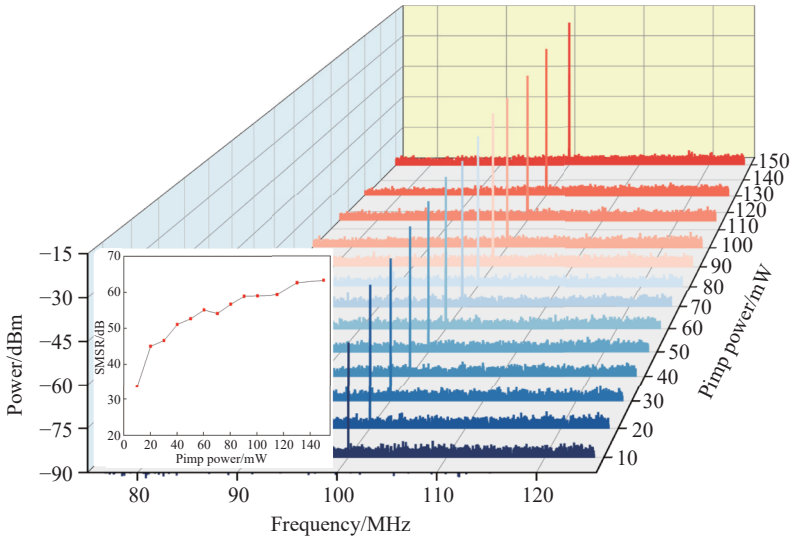

Fig. 8 The radio frequency spectra of the beat signals under different pump powers. Inset: SMSR evolution under different pump powers.

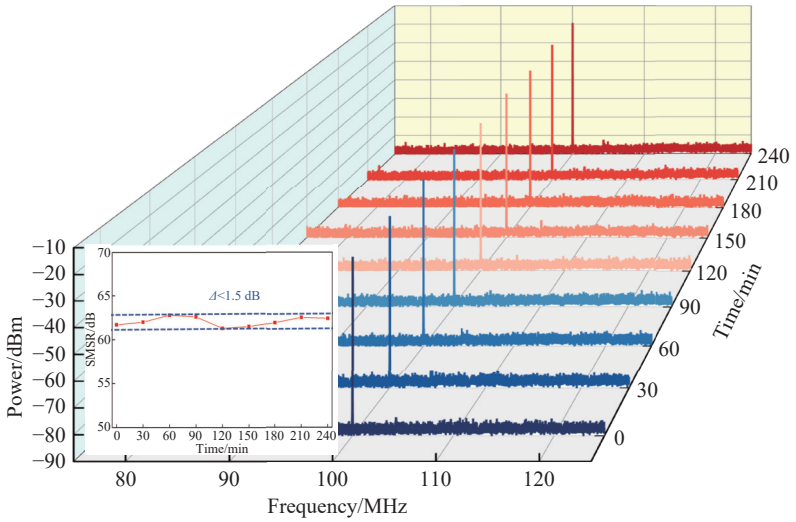

Fig. 9 The radio frequency spectra of the beat signals within 4 hours. Inset: SMSR fluctuation.

4.2 Optical spectrum

When the system reaches PT-symmetry breaking, its spectrum is simultaneously measured by OSA with a measurement bandwidth of 2 nm and a resolution of 0.02 nm. The evolution of the optical spectra at various pump power levels is shown in Fig. 10, with a central wavelength of 1 550.19 nm for the lasers. According to the inset of Fig. 10, the OSNR increases with increasing pump power, reaching 64.32 dB at 150 mW. To demonstrate the long-term stability of the system, the optical spectra of the laser are measured by the OSA over a 4-hour period, as shown in Fig. 11(a). The wavelength and output power fluctuations are maintained within 0.02 nm and 0.1 dB, respectively, as shown in Fig. 11(b).

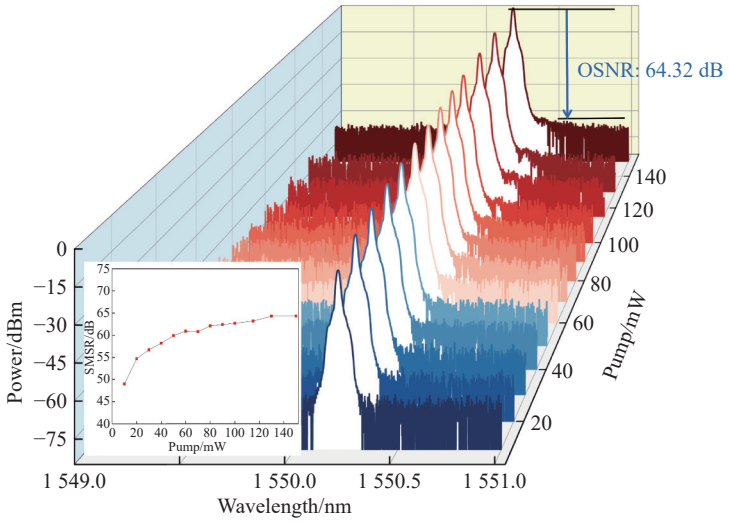

Fig. 10 Optical spectra evolution under different pump powers. Inset: OSNR evolution under different pump powers.

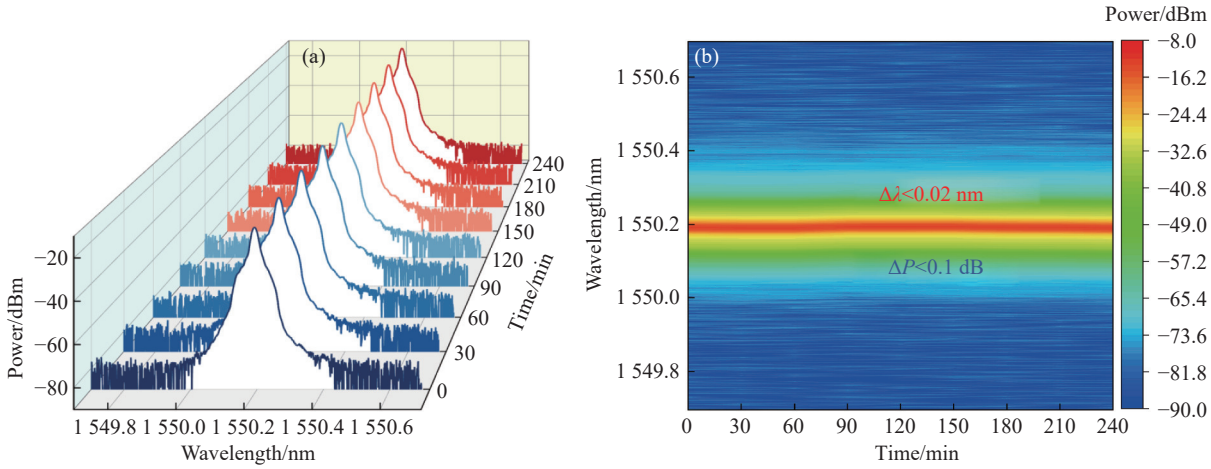

Fig. 11 The laser output characteristics within 4 hours. (a) Optical spectra, (b) stability of the laser output power and wavelength.

4.3 Linewidth

To verify the narrow linewidth of the fiber laser, the frequency spectrum bandwidth is set to 100 kHz. The measurement result is shown in Fig. 12.

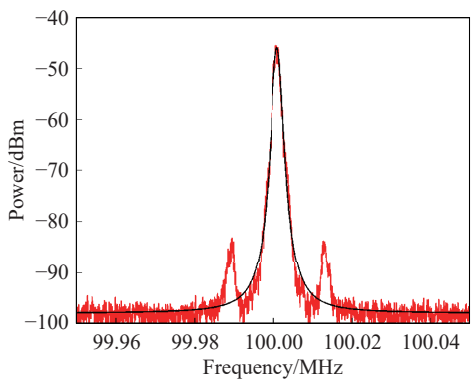

Fig. 12 The linewidth measurement and Lorentz fitting curve of the PT-symmetric laser.

The laser linewidth at 20 dB is 3.65 kHz by the Lorentzian fitting of the beat-frequency signals. The corresponding Lorentzian linewidth of the laser is calculated to be approximately 182.5 Hz. Environmental factors, such as temperature drift and mechanical vibrations, may induce significant linewidth broadening in the absence of active stabilization. Therefore, the intrinsic linewidth may be narrower.

4.4 Polarization properties

As depicted in Fig. 13, the polarization characteristics of the laser are continuously monitored for 4 hours by a polarization extinction ratio meter (ERM-101, General Photonics). The DOP is higher than 99.8%. The PER is greater than 30.8 dB, with fluctuations within a narrow range of less than 0.87 dB. These results indicate that the laser main-

tains stable linear polarization for 4 hours.

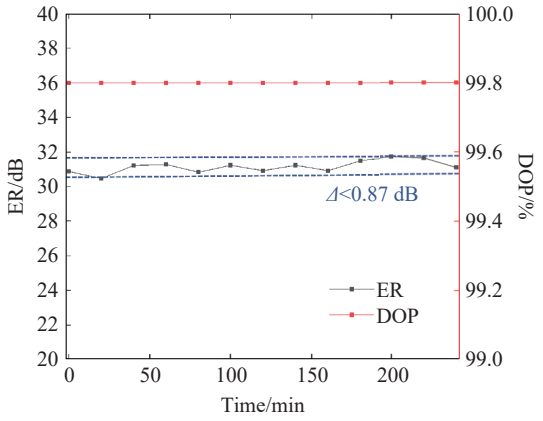

Fig. 13 Polarization stability of the PT-symmetric laser.

4.5 Noise analysis

T The RIN and phase noise of the PT-symmetric SLM laser are characterized and compared with those of several other lasers, including a home-built SA fiber SLM laser, a commercial fiber laser (Koheras BASIK X15, NKT Photonics), and a semiconductor laser (RIO, Orion laser module). The measurement of phase noise uses an interferometric sensor phase shift demodulation technique based on a 3 × 3 coupler and ellipse fitting algorithm (EFA)[22]. In this work, both the RIN and the phase noise are expressed in dB/Hz.

As depicted in Fig. 14, the relaxation oscillation peak of PT-symmetric laser is reduced by 17 dB relative to SA laser. The difference in the peak frequency of relaxation oscillations is mainly determined by factors such as the pump power, intracavity loss, and effective cavity length within the laser. Furthermore, as shown in Fig. 14(a), the PT-symmetric laser exhibits a reduction in RIN of more than 5 dB compared to the SA laser across the frequency range from 500 Hz to 10 kHz. In conventional SA lasers[23], the formation of standing-wave-induced dynamic gratings leads to the emergence of weak side modes. These side modes can deteriorate the laser's noise performance by introducing additional noise sources. Furthermore, dynamic gratings induce fluctuations in intracavity losses of the laser, thereby introducing additional noise. However, in PT-symmetric lasers, when the condition for PT-symmetry breaking is met, the gain contrast is markedly enhanced. As a result, the main mode experiences gain enhancement, leading to improved stability. This mechanism also contributes to the suppression of RIN in the PT-symmetric laser. When PT-symmetry breaking occurs, the system is forced to lock onto a single polarization mode. This polarization-stabilized configuration enhances robustness against environmental disturbances and effectively suppresses laser noise. Moreover, across the measured 10 Hz to 100 kHz range, the PT-symmetric laser exhibits lower RIN than the commercial NKT laser at all frequencies except the relaxation oscillation peak. Specifically, its noise level in the flat spectral region is about 18 dB lower, as shown in Fig. 14(b).

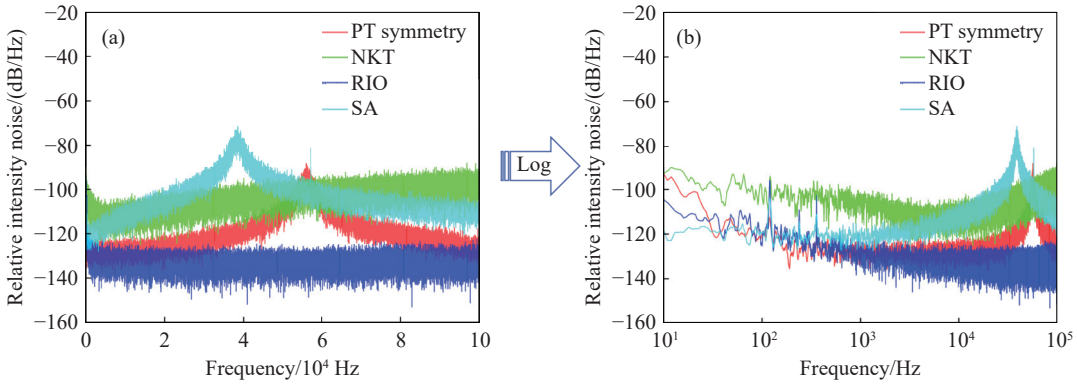

Fig. 14 RINs measurement for different lasers. (a) linear frequency scale; (b) logarithmic frequency scale.

In phase noise measurements, fiber lasers exhibit lower phase noise, as shown in Fig. 15. Overall, the PT-symmetric laser demonstrates superior noise performance compared to its fiber laser coun-

terparts, characterized by a lower RIN, particularly across the range of 10 Hz to 10 kHz. Notably, the PT-symmetric laser operates without encapsulation vibration-isolation devices, in contrast to the SA and NKT lasers. This result indicates that the PT-symmetric laser design offers improved stability and stronger resistance to environmental perturbations.

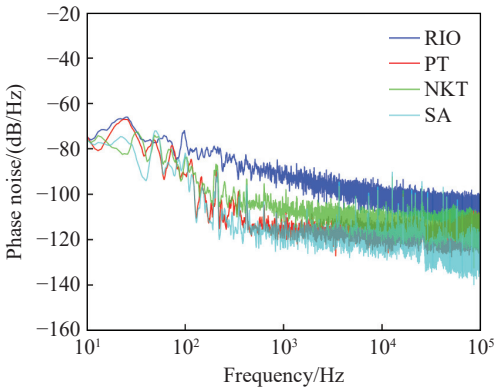

Fig. 15 Phase noise measurement for different lasers.

Semiconductor lasers typically exhibit lower RIN than fiber-laser counterparts. Nevertheless, as illustrated in Fig. 14, the PT-symmetric laser demonstrates a comparable RIN level to the semiconductor laser, except for the relaxation oscillation frequency. In addition, compared with semiconductor laser, the PT-symmetric laser exhibits a phase noise reduction of more than 10 dB across the frequency range from 100 Hz to 100 kHz, as shown in Fig. 15. Therefore, the PT-symmetric laser can simultaneously achieve the dual advantages of low relative intensity noise and low phase noise.

4.6 Wavelength-tuning

To achieve a SLM laser with wide-range wavelength tuning, the SM-FBG is replaced. A single-mode fiber mirror is used to provide reflection, and a PM-TOBPF (OTF-350, Santec) is incorporated into the main ring cavity to tune wavelength, as shown in Fig. 16. The pump power is set at 150 mW. Fig. 17(a) and 17(b) display the optical spectra obtained by adjusting the PM-TOBPF with different step sizes during SLM operation. A wavelength tuning range of 59 nm, from 1 516 nm to 1 575 nm, is achieved with peak power fluctuations maintained within 3 dB.

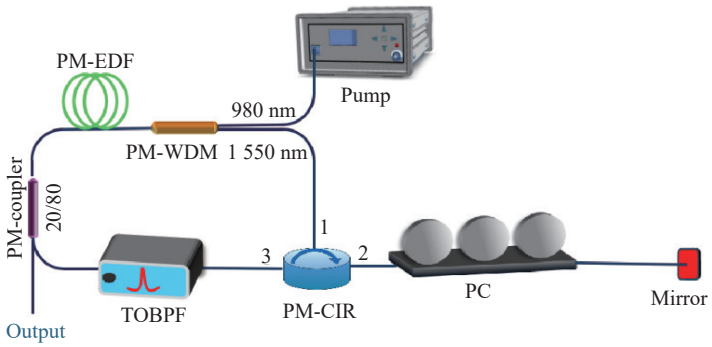

Fig. 16 Experimental setup of tunable SLM laser.

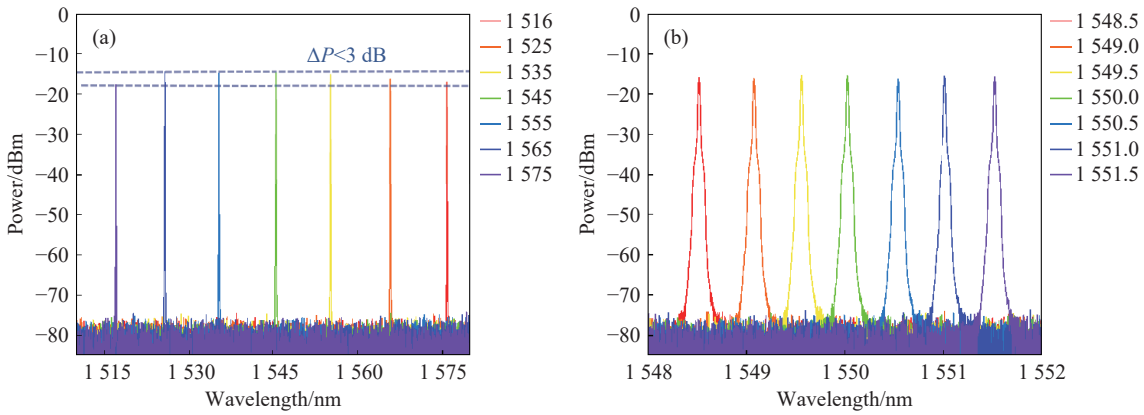

Fig. 17 (a) Optical spectra of SLM operation when the filter is tuned. The tuning range spans from 1 516 nm to 1 575 nm, with a step size of 10 nm. (b) The tuning range extends from 1 548.5 nm to 1 551.5 nm, with a step size of 0.5 nm.

It is evident that PT-symmetric mode selection stimulates a stable resonant mode for all wavelengths. However, the tuning range is constrained due to the gain bandwidth of the EDF and the operational bandwidth of the device.

4.7 Discussion

To further evaluate the advantages of the proposed laser, a comparison with representative PT-symmetric and conventional SLM fiber lasers is summarized in Table 1. As shown in the table, previously reported PT-symmetric lasers mainly focused on mode selection, SMSR, OSNR, or linewidth, whereas polarization characteristics, long-term stability, and noise behavior were rarely reported in a systematic manner. In contrast, the proposed laser achieves a high SMSR of 62.6 dB, a high OSNR of 64.32 dB, and a narrow linewidth of 182.5 Hz. Meanwhile, stable linearly polarized output is obtained, with a DOP of 99.8% and a PER of 30.8 dB. The proposed laser also shows good operational stability, with the power fluctuation and wavelength fluctuation remaining below 0.1 dB and 0.02 nm, respectively, together with additional noise analysis. Compared with the conventional SLM fiber laser listed in Table 1, the proposed PT-symmetric scheme shows a more favorable overall performance in linewidth, spectral purity, and polarization characteristics. These results indicate that the proposed PT-symmetric laser provides a favorable balance among stable SLM operation, narrow linewidth, polarization stability, and low-noise performance. It should be noted that the compared results were obtained from different laser structures and measurement conditions; therefore, the comparison is intended as a representative benchmark rather than a strictly one-to-one experimental evaluation.

Tab. 1 Comparison of the proposed laser with representative PT-symmetric and other SLM fiber lasers.

Type[Ref.]	SMSR	OSNR	Linewidth	Polarization	Stability	Noise analysis
PT-symmetric[13]	47.9 dB	about 60 dB	2.4 kHz	NR	NR	No
PT-symmetric[15]	about 50 dB	41.9 dB	390 Hz	NR	NR	No
PT-symmetric[17]	53.2 dB	about 40 dB	sub-kHz	NR	$\Delta P<0.12$ dB	No
PT-symmetric[18]	33 dB	about 60 dB	368 Hz	NR	NR	No
Conventional SLM fiber laser[24]	<40 dB	55.74 dB	1.8 kHz	NR	$\Delta P<0.65$ dB $\Delta\lambda<0.016$ nm	No
This work	62.6 dB	64.32 dB	182.5 Hz	DOP:99.8% PER:30.8 dB	$\Delta P<0.1$ dB $\Delta\lambda<0.02$ nm	Yes

5 Conclusion

In this work, we have proposed and experimentally demonstrated a low-noise linear-polarization fiber laser, achieving PT symmetry through a linear reflective structure to realize its mode selection. The linear reflection structure enables precise matching and coupling of gain and loss polarimetric loops. By utilizing a single PC, precise tuning of system gain and loss can be achieved, enabling straightforward realization of stable PT symmetry through simple operations. This not only makes the SLM operation more stable, but also greatly improves practicability. The laser demonstrates an SMSR of 62.6 dB, an OSNR of 64.32 dB, a Lorentz linewidth of 182.5 Hz, a DOP exceeding 99.8%, and a PER greater than 30.8 dB. Additionally, it demonstrates stable operation within 4 hours. Moreover, it is observed that the PT-symmetric laser exhibits superior performance in terms of noise characteristics. This proves the excellent mode selection effect of PT symmetry in the linear reflection structure. Furthermore, by replacing the SM-FBG with a combination of a single-mode fiber mirror and a PM-TO-BPF, a wide tuning range of 59 nm is achieved.

References:

[1] CHEN X CH, DAI G Y, WU S H, *et al*.. Coherent high-spectral-resolution lidar for the measurement of the atmospheric Mie–Rayleigh–Brillouin backscatter spectrum[J]. *Optics Express*, 2022, 30(21): 38060-38076.

[2] ZHANG J J, YAO J P. Parity-time–symmetric optoelectronic oscillator[J]. *Science Advances*, 2018, 4(6): eaar6782.

[3] ZHANG J J, LI L ZH, WANG G Y, *et al*.. Parity-time symmetry in wavelength space within a single spatial resonator[J]. *Nature Communications*, 2020, 11(1): 3217.

[4] HU H, OXENLØWE L K. Chip-based optical frequency combs for high-capacity optical communications[J]. *Nanophotonics*, 2021, 10(5): 1367-1385.

[5] SUN H, WU K T, ROBERTS K. Real-time measurements of a 40 Gb/s coherent system[J]. *Optics Express*, 2008, 16(2): 873-879.

[6] HERVÁS J, RICCHIUTI A L, LI W, *et al*.. Microwave photonics for optical sensors[J]. *IEEE Journal of Selected Topics in Quantum Electronics*, 2017, 23(2): 327-339.

[7] PREDEHL K, GROSCHE G, RAUPACH S M F, *et al*.. A 920-kilometer optical fiber link for frequency metrology at the 19th decimal place[J]. *Science*, 2012, 336(6080): 441-444.

[8] TSUKAMOTO S, LY-GAGNON D S, KATOH K, *et al*. . Coherent demodulation of 40-Gbit/s polarization-multiplexed QPSK signals with 16-GHz spacing after 200-km transmission[C]. *Optical Fiber Communication Conference and Exposition and the National Fiber Optic Engineers Conference*, Optica Publishing Group, 2005: PDP29.

[9] GUAN X CH, YANG CH SH, QIAO T, *et al*.. High-efficiency sub-watt in-band-pumped single-frequency DBR Tm^{3+}-doped germanate fiber laser at 1950 nm[J]. *Optics Express*, 2018, 26(6): 6817-6825.

[10] LI Y J, HUANG L G, GAO L, *et al*.. Optically controlled tunable ultra-narrow linewidth fiber laser with Rayleigh backscattering and saturable absorption ring[J]. *Optics Express*, 2018, 26(21): 26896-26906.

[11] ZHANG J L, YUE CH Y, SCHINN G W, *et al*.. Stable single-mode compound-ring erbium-doped fiber laser[J]. *Journal of Lightwave Technology*, 1996, 14(1): 104-109.

[12] HAO L Y, WANG X H, JIA K P, *et al*.. Narrow-linewidth single-polarization fiber laser using non-polarization optics[J]. *Optics Letters*, 2021, 46(15): 3769-3772.

[13] LI L ZH, CAO Y, ZHI Y Y, *et al*.. Polarimetric parity-time symmetry in a photonic system[J]. *Light: Science & Applications*, 2020, 9(1): 169.

[14] FAN ZH Q, ZHANG W F, QIU Q, *et al*.. Observation of PT-symmetry in a fiber ring laser[J]. *Optics Letters*, 2020, 45(4): 1027-1030.

[15] DAI ZH, FAN ZH Q, LI P, *et al*.. Widely wavelength-tunable parity-time symmetric single-longitudinal-mode fiber ring laser with a single physical loop[J]. *Journal of Lightwave Technology*, 2021, 39(7): 2151-2157.

[16] FAN ZH Q, DAI ZH, QIU Q, *et al*.. Parity-time symmetry in a single-loop photonic system[J]. *Journal of Lightwave Technology*, 2020, 38(15): 3866-3873.

[17] DAI ZH, WANG ZH R, YAO J P. Dual-loop parity-time symmetric system with a rational loop length ratio[J]. *Optics Letters*, 2023, 48(1): 143-146.

[18] DENG ZH P, LI L ZH, ZHANG J J, *et al*.. Single-mode narrow-linewidth fiber ring laser with SBS-assisted parity-time symmetry for mode selection[J]. *Optics Express*, 2022, 30(12): 20809-20819.

[19] LIU Y, WANG L Y, YOU Y J, *et al*.. Single longitudinal mode parity-time symmetric Brillouin fiber laser based on lithium niobate phase modulator Sagnac loop[J]. *Journal of Lightwave Technology*, 2023, 41(5): 1552-1558.

[20] LIU W L, WANG M G, YAO J P. Tunable microwave and sub-terahertz generation based on frequency quadrupling using a single polarization modulator[J]. *Journal of Lightwave Technology*, 2013, 31(10): 1636-1644.

[21] ULRICH R, RASHLEIGH S C, EICKHOFF W. Bending-induced birefringence in single-mode fibers[J]. *Optics Letters*, 1980, 5(6): 273-275.

[22] SHI J H, GUANG D, LI SH L, *et al*.. Phase-shifted demodulation technique with additional modulation based on a 3×3 coupler and EFA for the interrogation of fiber-optic interferometric sensors[J]. *Optics Letters*, 2021, 46(12): 2900-2903.

[23] WANG Q, SONG H Q, WANG X P, *et al*.. Experiments and analysis of tunable monolithic 1-μm single-frequency fiber lasers with loop mirror filters[J]. *Optics Communications*, 2018, 410: 884-888.

[24] HSU C H, LAI Y T, CHEN L Y, *et al*.. Tunable and stable single-frequency fiber laser by applying Rayleigh feedback light and saturable absorber filter[J]. *Optical Fiber Technology*, 2023, 79: 103333.

Author Biographies:

LIN zihan (2001—) received the B.S. degree in optoelectronic information science and engineering from Yangzhou University, Yangzhou, China, in 2023. His current research interests include fiber lasers. E-mail: 1814098694@qq.com

CAO Zhigang (1981—) received his Ph.D. in Physics and Electronics from Anhui University in 2015. Currently mainly engaged in research related to fiber sensors and fiber lasers. E-mail: caozhigang@ahu.edu.cn